Low-density anomalies and sub-Alfvénic solar wind

A. V. Usmanov,[1,2] M. L. Goldstein,[1] K. W. Ogilvie,[3] W. M. Farrell,[4] and G. R. Lawrence[5]

Received 22 July 2004; revised 14 September 2004; accepted 9 November 2004; published 28 January 2005.

[1] During 10–12 May 1999, the solar wind density dropped to an anomalously low value of $\sim$0.1 cm^{-3}. The density depletion occurred in the midst of relatively slow wind flow, in between faster flows, and was apparently associated with neither a coronal mass ejection nor a fast corotating stream. While the magnetic field intensity did not show any notable variation across the density depletion, plasma analyzers on the ACE and Wind spacecraft revealed an abnormally strong nonradial flow component with an azimuthal speed that peaked at $\sim$100 km s^{-1}. *Usmanov et al.* [2000b] suggested that the density anomaly was, in fact, a rarefaction at the trailing edge of relatively fast flow that formed as a result of suppression of coronal outflow from a region that earlier provided fast wind flow. The suppression in turn may have resulted from a rapid restructuring of solar magnetic fields during the polar field reversal. Here we show results from a two-dimensional time-dependent MHD simulation applied to the helioequatorial plane. The initially longitude-independent Parker solar wind and Archimedean spiral magnetic field are disturbed by a low-velocity/high-density jump on an inner computational boundary at 20 $R_\odot$. We follow the development and propagation of the rarefaction to Earth orbit and compare pseudo-time series with near-Earth spacecraft measurements. We show that a strong rarefaction can develop behind the fast flow and that simulation results and spacecraft observations are generally in agreement. The simulated radial magnetic field shows a relatively small variation across the density anomaly compared with that of the density. The stream interaction generates strong azimuthal velocities in the slow flow region, as observed. The simulation shows a sub-Alfvénic flow region embedded within the low-density region that does not extend all the way back to the Sun but which has become disconnected as the depletion propagates to Earth orbit. We discuss also the correlation between low-density and sub-Alfvénic events in the solar wind as inferred from spacecraft observations using the OMNI 2 data set from 1963 to 2003.

Citation: Usmanov, A. V., M. L. Goldstein, K. W. Ogilvie, W. M. Farrell, and G. R. Lawrence (2005), Low-density anomalies and sub-Alfvénic solar wind, *J. Geophys. Res.*, *110*, A01106, doi:10.1029/2004JA010699.

1. Introduction

[2] On 10–12 May 1999, the ACE and Wind spacecraft observed extremely rarefied solar wind with a density that fell to $\sim$0.1 cm^{-3}. The density depletion was embedded within slow wind flow; $V_{sw} \lesssim 350$ km s^{-1}. The flow was also highly nonradial, deviating by up to $\sim$20° toward the direction of Earth's orbital motion [*Usmanov et al.*, 2000b]. Surprisingly, the magnetic field showed little if any variation during the event; however, a sector boundary was observed shortly thereafter. The exceptionally low densities produced unusually low Alfvén Mach numbers and, combined with the low speed, caused the solar wind ram pressure to drop to $\sim$0.02 nPa ($\sim$1% of its typical value). This pressure drop along with the low Alfvén Mach numbers profoundly affected the Earth's magnetosphere and caused the bow shock to inflate to the orbit of the Moon [*Lazarus*, 2000; *Fairfield et al.*, 2001]. Another extraordinary aspect of the event was that the solar wind speed dropped below the Alfvén speed, i.e., the solar wind became sub-Alfvénic for at least 2 hours. Interplanetary scintillation (IPS) observations of the interplanetary plasma during this time period [*Balasubramanian et al.*, 2003; see also *Vats et al.*, 2001] showed that solar wind densities at heliocentric distances from 0.2 to 1 AU were globally reduced and that the decrease was accompanied by a noticeable drop in solar wind speed. *Smith et al.* [2001, 2004] found that in addition to the nearly constant magnetic field, the "void" had an unusually low level of magnetic fluctuations, suggesting its relative isolation from sources of such fluctuations.

[3] The density of steady solar wind is usually inversely correlated with its velocity: slow wind is associated with the

[1]Interplanetary Physics Branch, Laboratory for Extraterrestrial Physics, NASA Goddard Space Flight Center, Greenbelt, Maryland, USA.
[2]Institute of Physics, St. Petersburg State University, St. Petersburg, Russia.
[3]Laboratory for Extraterrestrial Physics, NASA Goddard Space Flight Center, Greenbelt, Maryland, USA.
[4]Planetary Magnetospheres Branch, Laboratory for Extraterrestrial Physics, NASA Goddard Space Flight Center, Greenbelt, Maryland, USA.
[5]Department of Solar Physics, Royal Observatory of Belgium, Brussels, Belgium.

0148-0227/05/2004JA010699

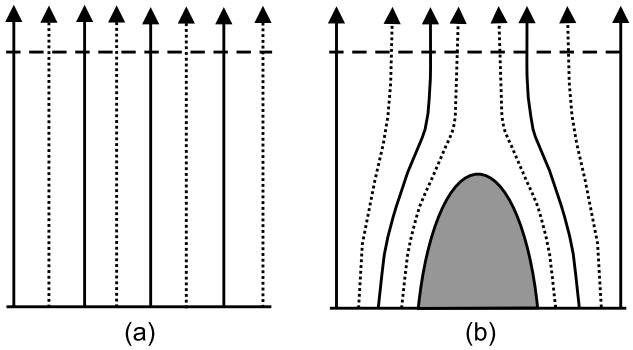

Figure 1. Schematic of a change in boundary conditions near the Sun that might produce a low-density anomaly. Magnetic field lines are shown with the solid lines and flow lines with the dashed lines.

heliospheric plasma sheet and is therefore relatively dense; fast wind, which originates in coronal holes, is usually more tenuous. A consequence of this anticorrelation is that the mass flux is much less variable than either speed or density alone [*Phillips et al.*, 1996; *McComas et al.*, 2000]. Owing to solar rotation, fast and slow flows can become radially aligned and can then interact to produce "corotating interaction regions" (CIRs) consisting of a compression region at the trailing edge of the slow stream and a rarefaction region at the trailing edge of the fast stream [e.g., *Hundhausen*, 1972; *Pizzo*, 1978]. Compressions and rarefactions are also generated by transient flows such as coronal mass ejections (CMEs), explosive releases of material from the corona that propagate like pistons through slower ambient wind and create compression regions by accumulating the material ahead of them and leaving rarefactions behind [e.g., *Gosling*, 2000]. The rarefaction of May 1999 appears to be associated with neither a CIR nor a CME [*Richardson et al.*, 2000].

[4] *Usmanov et al.* [2000b] found that the low-density event of 10–12 May 1999 occurred just at the beginning of a period of the polar field reversal on the Sun. They suggested that the quick restructuring, which is characteristic of periods of field reversal, could lead to a suppression of the coronal outflow from the region that had earlier served as a source of relatively fast flow and could also lead subsequently to the density depletion that inevitably builds up if a fast flow is followed by slow flow. Coronal magnetic field maps from the Wilcox Solar Observatory at Stanford appear to support this idea by revealing a latitudinal excursion of the neutral line (which is usually associated with a source of slow wind near the heliospheric plasma sheet) across the helioequator at appropriate longitudes [see *Usmanov et al.*, 2000b].

[5] A schematic picture to explain the basic idea which we will further exploit in present paper is shown in Figure 1. The left panel depicts an initial configuration with the straight magnetic field and plasma flow lines. We assume that the initial state transforms into the configuration shown in the right panel due to emergence of a new active region with bipolar magnetic field. The latter pattern is similar to that of a coronal streamer [e.g., *Pneuman and Kopp*, 1971] except that the magnetic field does not change polarity above the closed field region. Plasma is flowing around this region and forms a sheet of slower and more dense material above it. The mass and magnetic fluxes are redistributed by tangential flows so that the magnetic field and mass fluxes at the outer boundary are much more constant than are the density or speed [*Usmanov et al.*, 2000a]. If the transformation between the patterns shown in Figure 1 occurs quickly, we can expect a strong rarefaction to develop as a result of the drop in outflow speed above the newly created region of closed magnetic field.

[6] In the present paper we use MHD simulations to investigate the hypothesis that such a mechanism (which we will refer to as a "coronal outflow suppression") could be responsible for the very strong and long-duration rarefaction of May 1999. We solve the two-dimensional time-dependent MHD equations to simulate the propagation of a slow wind stream through a faster background and the subsequent development of a density depletion in front of the slow stream. It is important to note that in the present study we do not initialize the transient disturbance by simulating the transformation between the patterns shown in the left- and right-hand panels of Figure 1, but instead we place our inner boundary at $r = 20\ R_\odot$ ($R_\odot$ is the solar radius), which is well above the top of the patterns, and study the effects of a low-velocity/high-density jump at this boundary. We show that a strong rarefaction with an embedded sub-Alfvénic region can indeed develop on the trailing edge of a fast stream. Our comparison of the results of the simulations with spacecraft data shows general agreement both in plasma and magnetic field parameters.

[7] Starting from the pioneering work of *Hundhausen and Gentry* [1969], numerous MHD studies have targeted propagation of transients through the ambient solar wind. In two- and three-dimensions such studies were carried out by, e.g., *De Young and Hundhausen* [1971], *Nakagawa and Wellck* [1973], *Wu et al.* [1983], *Han et al.* [1988], *Mikić and Linker* [1994], *Usmanov and Dryer* [1995], *Riley et al.* [1997], *Hu* [1998], *Wu et al.* [1999], *Odstrčil and Pizzo* [1999], *Groth et al.* [2000], *Odstrčil et al.* [2002], and *Manchester et al.* [2004]. A common feature of all those studies is that they all considered propagation of fast streams through slower backgrounds. Our approach is different in that we deal with the evolution of a slow stream on a faster background. A similar idea was exploited by *Gosling and Skoug* [2002] to explain events wherein the interplanetary magnetic field at a fixed point in space remained nearly radial for many hours. To our knowledge, the only computational effort with a slower transient on faster background was that of *Gosling and Riley* [1996], who simulated the acceleration of a slow CME by faster ambient wind in one dimension.

[8] It is extremely unusual for M_A to be less than 1, where M_A is the Alfvén Mach number. Observations near 1 AU show that solar wind is typically highly super-Alfvénic. It is only on very rare occasions that the number has dropped to the values of order 1 and below. In particular, *Gosling et al.* [1982] showed that during the low-density events of 4 July, 31 July, and 22 November 1979, the solar wind became sub-Alfvénic. In this study we have used the recently released OMNI 2 spacecraft data compilation for 1963–2003 to select intervals with abnormally low densities and $M_A < 1$. We also discuss the apparent correlation between minimum M_A and minimum densities for the selected events.

[9] The outline of the paper is as follows: In section 2 we describe the governing equations and discuss in detail the initial and boundary conditions used. The simulation results, including comparison of pseudo-time series with near-Earth spacecraft observations, are presented and discussed in section 3. Section 4 is dedicated to the selection and analysis of spacecraft data for the low-density and sub-Alfvénic events for the entire space era; this section presents also contour maps describing the May 1999 event in terms of the simulated Alfvén Mach number. Concluding remarks are given in section 5.

2. Model Formulation

[10] We describe solar wind plasma by single-fluid, polytropic MHD equations in the frame of reference corotating with the Sun and assume that dissipation is negligible. In a time-dependent formulation, the two-dimensional equations adjusted for the solar equatorial plane are [see, e.g., *Nakagawa and Wellck*, 1973]

$$\frac{\partial}{\partial t}\left(r^2\rho\right) = -\frac{\partial}{\partial r}\left(r^2\rho u_r\right) - \frac{\partial}{\partial \phi}\left(r\rho v_\phi\right), \tag{1}$$

$$\begin{aligned}\frac{\partial}{\partial t}\left(r^2\rho u_r\right) = & -\frac{\partial}{\partial r}\left[r^2\left(\rho u_r^2 + P + \frac{B_\phi^2 - B_r^2}{8\pi}\right)\right] \\ & - r\frac{\partial}{\partial \phi}\left(\rho u_r v_\phi - \frac{B_r B_\phi}{4\pi}\right) \\ & + r\left(\rho u_\phi^2 - \frac{\rho G M_\odot}{r} + 2P + \frac{B_r^2}{4\pi}\right),\end{aligned} \tag{2}$$

$$\begin{aligned}\frac{\partial}{\partial t}\left(r^2\rho u_\phi\right) = & -\frac{\partial}{\partial r}\left[r^2\left(\rho u_r u_\phi - \frac{B_r B_\phi}{4\pi}\right)\right] \\ & - r\frac{\partial}{\partial \phi}\left(\rho u_\phi v_\phi + P + \frac{B_r^2 - B_\phi^2}{8\pi}\right) \\ & - r\left(\rho u_r u_\phi - \frac{B_r B_\phi}{4\pi}\right),\end{aligned} \tag{3}$$

$$\frac{\partial}{\partial t}\left(rB_r\right) = -\frac{\partial}{\partial \phi}\left(v_\phi B_r - u_r B_\phi\right), \tag{4}$$

$$\frac{\partial}{\partial t}\left(rB_\phi\right) = \frac{\partial}{\partial r}\left[r\left(v_\phi B_r - u_r B_\phi\right)\right], \tag{5}$$

$$\frac{\partial}{\partial t}\left(r^2 P^{1/\gamma}\right) = -\frac{\partial}{\partial r}\left(r^2 u_r P^{1/\gamma}\right) - r\frac{\partial}{\partial \phi}\left(v_\phi P^{1/\gamma}\right). \tag{6}$$

Equations (1)–(6) are written in spherical coordinates with the independent variables being the time t, heliocentric distance r, and longitude ϕ. The dependent variables are the mass density ρ, radial velocity u_r, azimuthal velocity v_ϕ, radial magnetic field B_r, azimuthal magnetic field B_ϕ, and thermal pressure P. In addition, the azimuthal velocity in the inertial frame is $u_\phi = v_\phi + \Omega r$, the number density $n = \rho/m_p$, the polytropic index is γ, the gravitational constant is G, the solar mass is $M_\odot$, the solar sidereal rotation rate is Ω, and the proton mass is m_p.

[11] We solve (1)–(6) numerically on a grid of 122 × 94 points logarithmically spaced in the r direction [*Usmanov*, 1993] from the inner boundary at 20 $R_\odot$ to 1 AU and uniformly spaced in the ϕ direction from $\phi = -3$ to 183°. The radial grid spacing increases linearly with r from 0.4 $R_\odot$ at the inner boundary to ~4 $R_\odot$ at 1 AU. The spacing in the azimuthal direction is 2°. For the polytropic index γ, we use the empirical value of 1.46 inferred by *Totten et al.* [1995] from Helios 1 observations.

[12] The ambient solar wind is assumed to be a radial, azimuthally uniform Parker-type flow permeated by spiral magnetic field. The reference values in the initial state at $r_0 = 20\ R_\odot$ are the radial velocity $u_0 = 350$ km s^{-1}, electron number density $n_0 = 1200$ cm^{-3}, temperature $T_0 = 1.25 \times 10^6$ K, and radial magnetic field $B_0 = 0.01$ G. Using these values, we integrated the steady one-dimensional equations for mass, momentum, energy, and magnetic flux conservation outward along radius to obtain the following values at 1 AU: $u_r = 472$ km s^{-1}, $n = 7.5$ cm^{-3}, $T = 1.15 \times 10^5$ K, and $B_r = 8.4$ nT. The azimuthal magnetic field B_ϕ is computed from the condition that velocity and magnetic field vectors are parallel in the frame of reference corotating with the Sun [*Weber and Davis*, 1967], i.e., $\mathbf{v} \| \mathbf{B}$ or $B_\phi/B_r = v_\phi/u_r$. (The fundamental assumption underlying this expression is the absence of an electric field in the frame of reference corotating with the Sun.) Provided that $u_\phi = 0$ in the initial state, $B_\phi = -\Omega r B_r/u_r$. Sonic speed at the inner boundary in the initial state $(\gamma k_B T_0/m_p)^{1/2}$, where k_B is the Boltzmann's constant, is ~120 km s^{-1} and the Alfvén speed $V_{A0} = B_0[(1 + \Omega^2 r_0^2/u_0^2)/4\pi\rho_0]^{1/2} \sim 630$ km s^{-1}. Thus the ambient wind near the inner boundary is supersonic but sub-Alfvénic. The resulting background solution is shown in Figure 2 and is used as the initial ($t = 0$) condition in our simulations of low-density transients.

[13] At $t \geq 0$, we introduce a localized finite strength disturbance on the lower radial boundary within a sector of 60° in longitude and centered at $\phi = 120°$. Figure 3 shows the variation of velocity and density imposed at $r = 20\ R_\odot$. The velocity perturbation is specified as

$$u_r = u_0 - \Delta u\left[\frac{\sin(\pi x)}{\pi x}\right],$$

where

$$x = \frac{\phi - \phi_0}{\Delta\phi}, \qquad |x| \leq 1,$$

$\Delta u = 300$ km s^{-1}, $\phi_0 = 120°$, and $\Delta\phi_0 = 30°$; that is, the velocity drops from 350 to 50 km s^{-1} in the center of the disturbance. We take the mass flux and plasma pressure P to be the same in the ambient and disturbed flows. Thus (1) the density anticorrelates with the velocity and peaks at ~84800 cm^{-3} to satisfy the constant mass flux condition $nu_r = n_0 u_0$, (2) the plasma temperature variation is similar to that of velocity so that $nT = n_0 T_0$. We assume also that the jump in the boundary conditions for u_r, n, and T is not instantaneous but takes 1 hour of linear change between the ambient wind and disturbed parameters. Similar to the plasma pressure P, B_r is kept fixed at the initial values for the entire simulation time. Meantime, because the flow is sub-Alfvénic at the boundary, one of the dependent variables should be determined from the

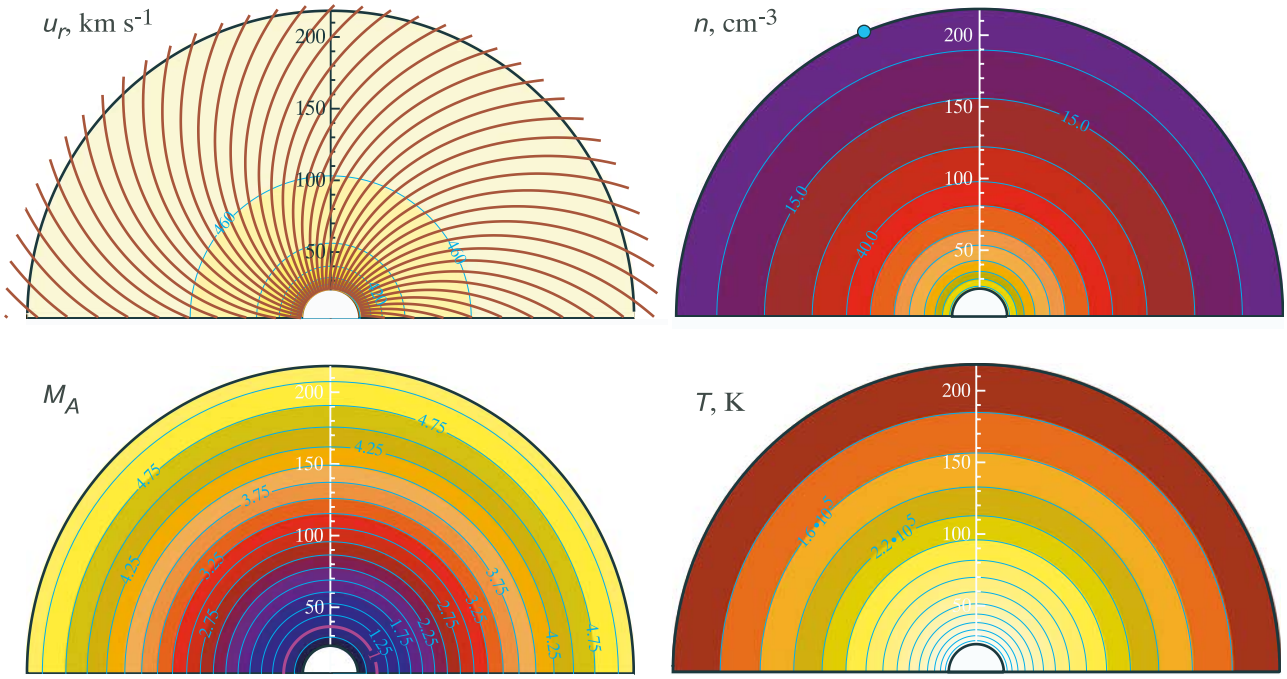

Figure 2. Contour plots of the radial velocity u_r, number density n, Alfvén Mach number M_A, and temperature T in the ambient solar wind at $t = 0^h$. The heliocentric distance is indicated in solar radii. The magnetic field lines are superimposed on the u_r map. The small circle on the outer boundary of the density map marks the assumed location of the Earth as discussed in section 3.

solution near the boundary using the so-called compatibility relation along the characteristic coming to the boundary [e.g., *Nakagawa and Steinolfson*, 1976; *Steinolfson and Dryer*, 1984]. It was shown by *Nakagawa and Steinolfson* [1976] that the compatibility relation can be successfully replaced by linear extrapolation back to the boundary. In the present work, we choose to obtain the boundary values of u_ϕ from the extrapolation. Finally, the boundary values of the azimuthal magnetic field B_ϕ are computed from the condition $\mathbf{v}\|\mathbf{B}$ in the rotating frame: $B_\phi = (u_\phi - \Omega r)B_r/u_r$.

[14] Periodic boundary conditions are imposed at the azimuthal edges of the mesh, while simple extrapolation of zeroth order for conservation variables is employed at the upper boundary at 1 AU. To integrate equations (1)–(6) from $t = 0$ to 256 hours, we apply the explicit TVD Lax-Friedrichs numerical scheme with the Woodward limiter [*Tóth and Odstrčil*, 1996]. The solenoidal condition for the magnetic field $\nabla \cdot \mathbf{B} = 0$ is maintained using the Tóth's field-interpolated central difference scheme [*Tóth*, 2000]. The computations reported below involve several thousand time steps and typically take about 20 min on a PC computer.

3. Simulation Results

[15] Figures 4–6 present our simulation results for the evolution of low-density transient generated by the jump to lower velocity/higher density conditions at the inner boundary. The contour maps of the radial velocity, u_r, number density, n, azimuthal velocity, u_ϕ, and plasma temperature, T, are shown for $t = 64$, 128, and 256 hours in the frame of reference rotating with the Sun. It is clearly seen that a rarefaction region forms as a result of the coronal flow suppression on the inner boundary. Low densities develop in the leading portion of slow wind bubble and the low-density region propagates outward relatively slowly, taking about 5 days to reach 1 AU. The depletion becomes deeper as it propagates outward.

[16] The contour plots of u_ϕ in Figures 4–6 show that the low-density region is associated with a strong velocity component in the corotation (i.e., positive in ϕ) direction. There are at least two mechanisms for the low-density low-speed transient to acquire momentum in this direction. The first and more obvious one is the pile-up of material at its trailing edge where slow transient material is radially aligned and is overtaken by faster ambient wind. To illuminate this effect, we ran the same code for a purely hydrodynamic case by setting the magnetic field (respon-

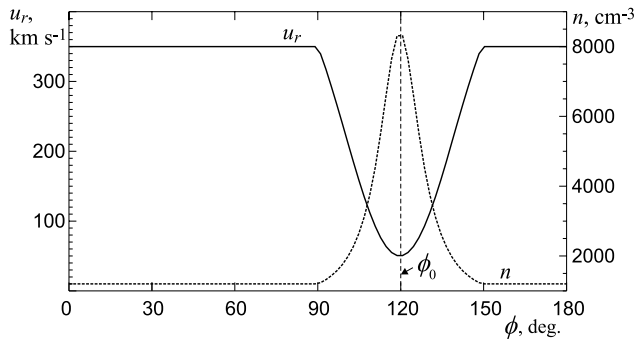

Figure 3. Longitudinal variations of the radial velocity u_r and number density n introduced at the inner boundary ($r = 20\ R_\odot$) at $t = 0$.

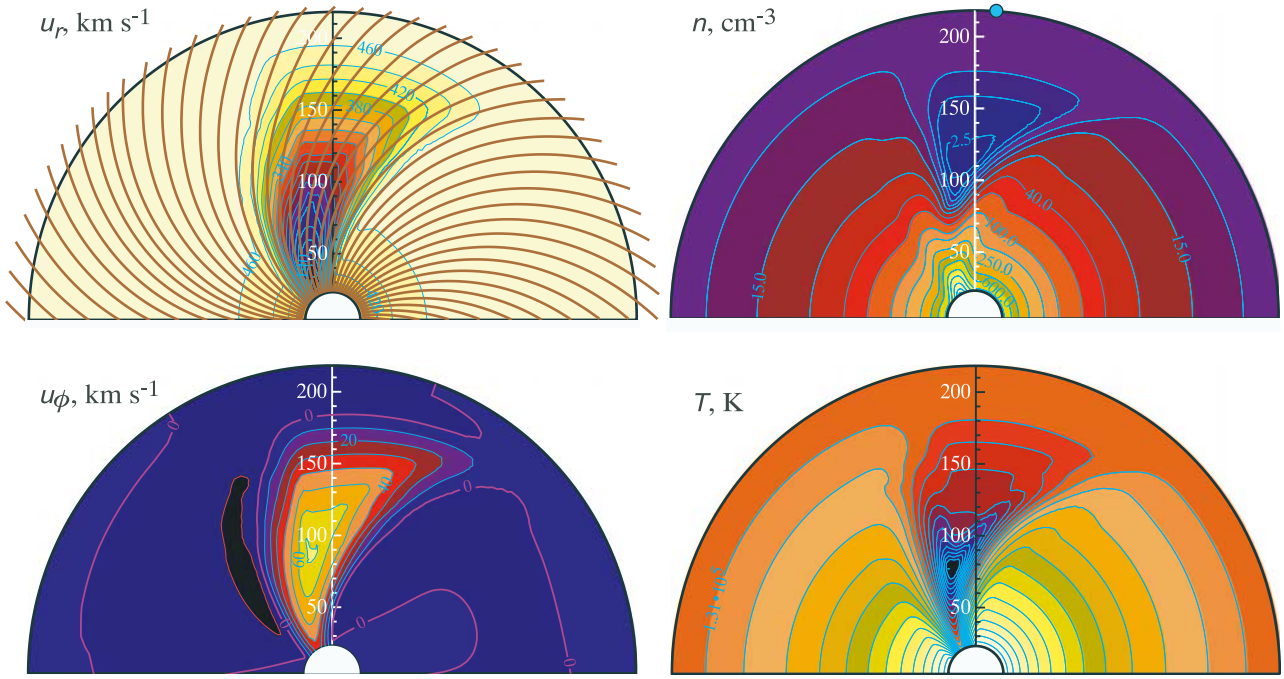

Figure 4. Contour plots of the radial velocity u_r, number density n, azimuthal velocity u_ϕ, and temperature T for $t = 64^h$. The heliocentric distance is indicated in solar radii. The magnetic field lines are superimposed on the u_r map. The small circle on the outer boundary of the density map marks the assumed location of the Earth.

sible for the second mechanism, see below) to zero. Figure 7 presents a color map of azimuthal velocity distribution at t = 64 hours for this case. One can see that the increased plasma pressure at the trailing edge of the transient produce nonradial flows in the corotation direction. These pressure-driven flows relieve the stresses built up by stream interaction and transport mass away from the compression region into the rarefaction region inside the transient [cf. *Pizzo*, 1978]. There exist also two regions of negatively directed flows which are relatively weaker. The first region forms behind the strongest compression at the trailing edge where the nonradial flows work to reduce pressure

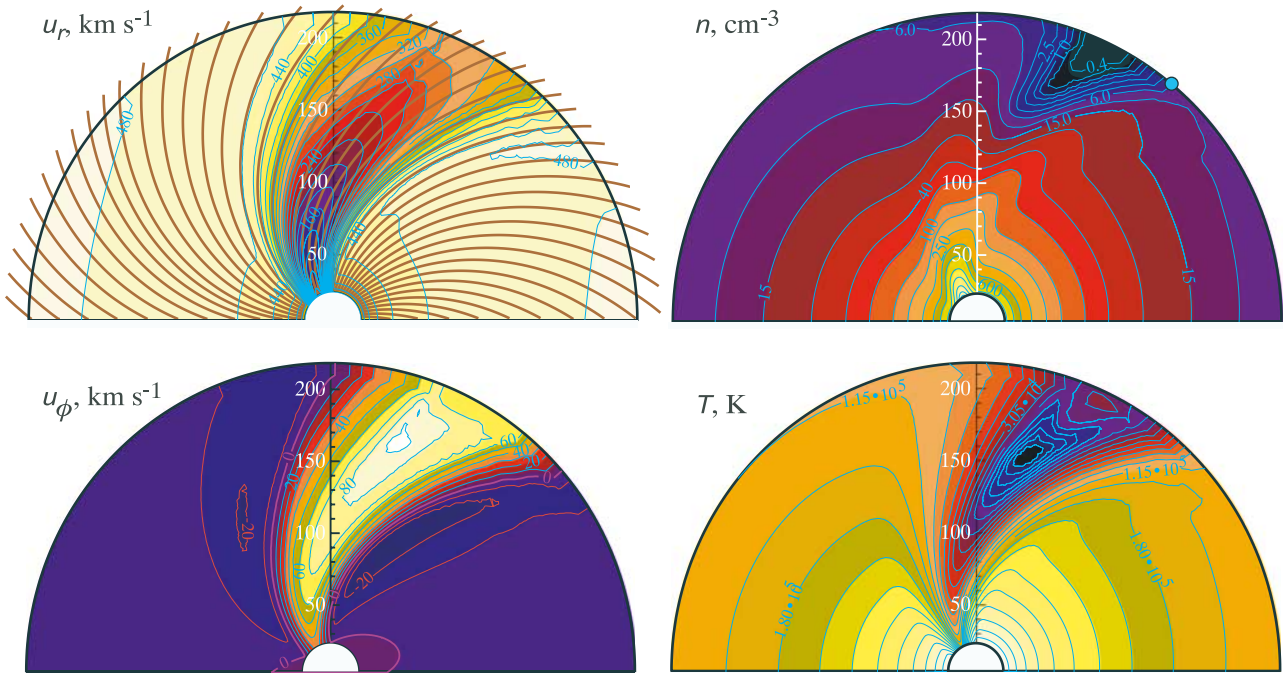

Figure 5. The same as in Figure 4 for $t = 128^h$.

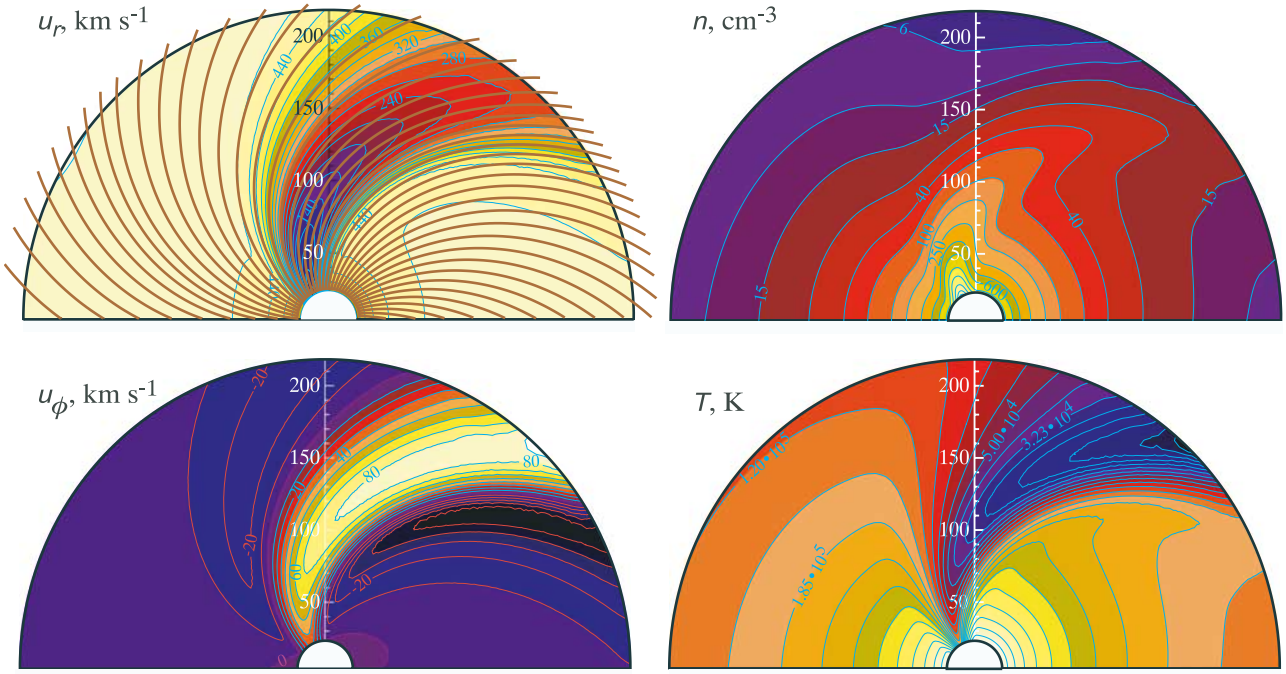

Figure 6. The same as in Figure 4 for $t = 256^h$.

gradients between the compression and the following ambient wind. The other extended region of negatively directed flows is associated with a pressure gradient between the ambient wind and following low-density transient.

[17] The second mechanism for generating a strong positive u_ϕ inside the transient is the following: Owing to the very low density of plasma, the effect of the magnetic field on the outstreaming flow is much more important than it is for the ambient wind. Calculation of the Alfvén Mach number (see Figure 11 in section 4 below) shows that the flow inside the transient is sub-Alfvénic so that the kinetic energy density is less than the magnetic energy density. This situation is similar to the one close to the Sun where the flow is sub-Alfvénic, the magnetic field is dominant, and the flow is forced to conform to the magnetic field. That means in particular that near the Sun the coronal plasma tends to corotate with the Sun [*Weber and Davis*, 1967]. The effect of corotation is most important inside the region where coronal outflow is sub-Alfvénic and then it drops with the distance to become very small by 1 AU ($\sim$1 km s^{-1} [see *Weber and Davis*, 1967]). The extension of the sub-Alfvénic regime into the distant solar wind by the low-density transient implies that the effect of corotation also extends much farther from the Sun than in typical solar wind. We believe that this effect is the second source of the strong azimuthal velocity within the transient that we see in Figures 4–6 and that was actually observed during the May 1999 event.

[18] Another prominent feature of the simulated transient in Figures 4–6 is the near absence of perturbations in magnetic field structure. The magnetic field preserves its initial Archimedean spiral form while responding to slow speeds within the transient by forming a slightly larger inclination of the lines of force to the radial direction. Clearly, this behavior is another consequence of the fact that the transient's magnetic energy density is of order or even higher than the kinetic energy density. This prevents magnetic field from significant distortion and is clearly unlike what happens in an opposite (i.e., usual) case when fast-moving transients plough into a low-speed background. In the latter case, the pile-up of material and magnetic field ahead of ejecta would lead to very sharp perturbations in the plasma and magnetic field parameters and to the formation of a shock [e.g., *Wu et al.*, 1983]. We have already noticed that spacecraft observations did not show any sharp variations in magnetic field during May 1999 event, so our simulation results appear to be in agreement with those observations.

[19] The modulations introduced near the Sun propagate outward to 1 AU in the form of a slow-moving low-density transient. Eventually, the transient drifts out of the computational domain leaving behind itself a slow-wind stream,

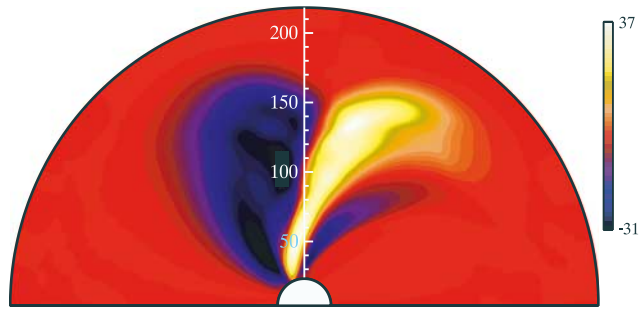

Figure 7. Results of a purely hydrodynamic run, i.e., the parameters are the same as in the previous run, but the magnetic field has been set to zero. The two-dimensional color contour of azimuthal component of velocity, u_ϕ, is shown at $t = 64^h$.

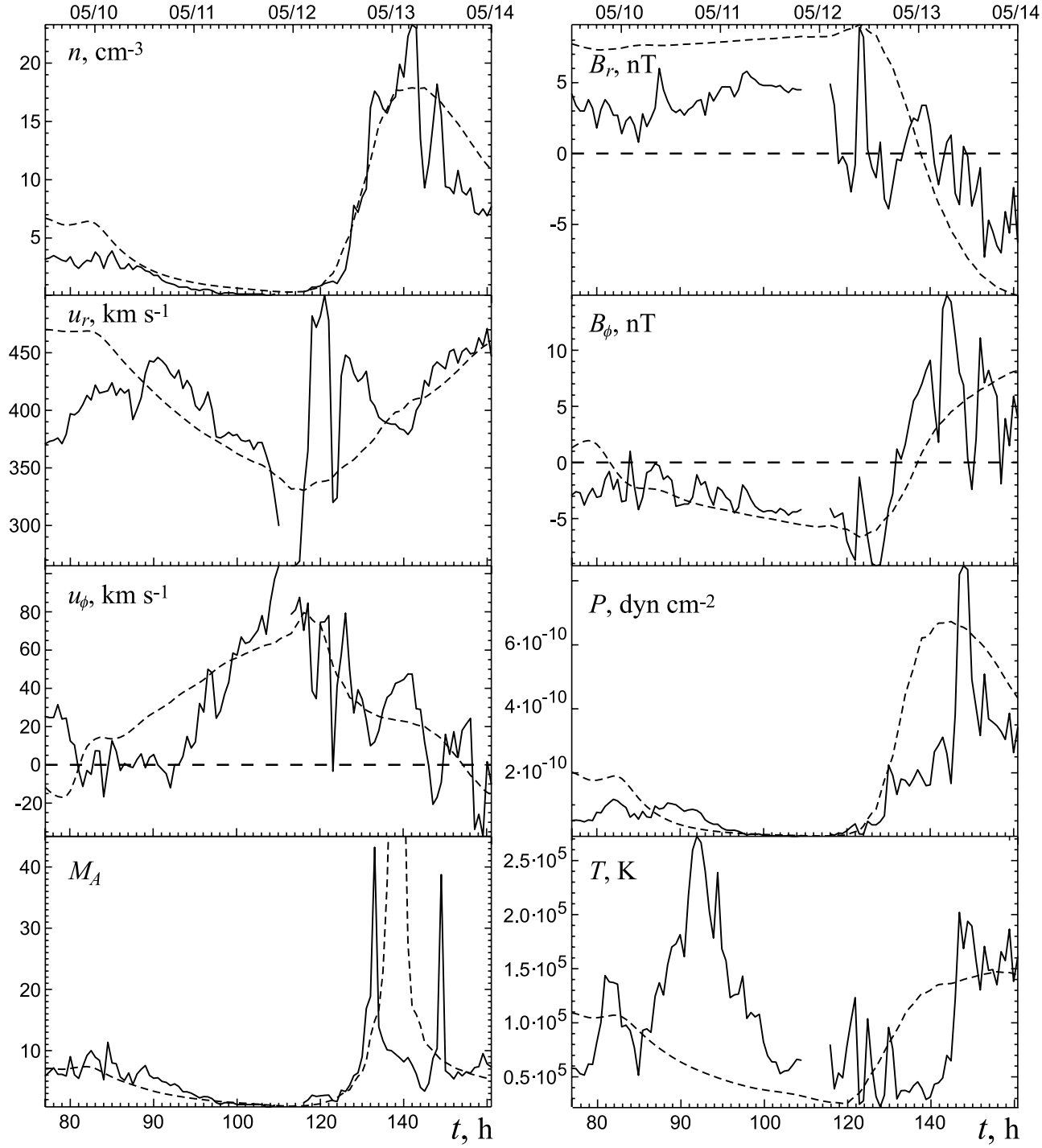

Figure 8. Comparison of OMNI 2 1-hour spacecraft data (solid lines) and simulated profiles (dashed lines) for a time interval around 10–12 May 1999 low-density anomaly.

which is steady in the rotating frame and corotates along with the ambient wind (see Figure 6). The entire process thus can be considered as the birth of a slow corotating stream from a faster background. A schematic and description of stream interaction for such corotating structure consisting of a slow wind flow in between faster flows was given by *Usmanov et al.* [2000b] (see their Figure 4).

[20] The results obtained thus far appear to be in qualitative agreement with observations during the May 1999 event. To attempt a more quantitative comparison, we modified our code by including a variation in B_r in the inner boundary and initial conditions so that the sector boundary observed on 12 May shortly after the density depletion could be reproduced. Instead of assuming a longitude-independent B_r, we chose it to have the form of $B_r = B_0(r/r_0)^2\tanh[(\phi - \phi_s)/\Delta\phi_s]$, that is with a smooth change of the sign at $\phi_s = 95°$ and with halfwidth of the transition $\Delta\phi_s = 10°$. The azimuthal magnetic field B_ϕ was

again set to be independent of longitude and to have a zero value in the initial state. Apart from the modified magnetic field, all other variables and conditions were the same as before.

[21] To superpose the results of the run with sector boundary and the data from Earth-orbiting spacecraft, we have to select values of two parameters: the position of the Earth with respect to the simulated transient and a time interval from the simulation run to compare with spacecraft observations. After numerous experiments with time delays and Earth's locations relative to the disturbance, we found that a best fit to spacecraft data corresponds to the initial position of Earth at $\phi = 112°$ (i.e., 8° east of the center of the disturbance) and to arrival of the depletion to Earth's vicinity at $t \sim 90$ hours after initialization of the disturbance. The Earth's initial location (see Figure 2) determines its trajectory as it moves through the propagating disturbance (see Figures 4–6) due to solar rotation and its own (relatively slow) orbital movement, while the choice of time interval serves for synchronization of the time series simulated and observed.

[22] Figure 8 shows simulated profiles versus OMNI 2 hourly averaged data. In general the computed profiles bear some resemblance to the observations. In particular, the overall pattern of density, consisting of the strong rarefaction and subsequent compression, and also its duration and intensity are reproduced fairly well. The rarefaction-compression pattern corresponds to a "valley" perturbation in the radial velocity with a leading near-linear decrease from 470 to 330 km s^{-1} during the rarefaction and following symmetric recovery during the compression phase. On the whole, the simulated variation of u_r seems to be similar to that measured with the striking exception of a "wave-packet" variation with two higher-speed streams observed on 12 May which clearly drops out of the "valley" pattern and have no explanation in frame of our simulation example. The computed azimuthal velocity u_ϕ peaks at ~80 km s^{-1} and its pattern roughly resembles spacecraft data.

[23] A similar degree of resemblance is evident for the magnetic field components, with a somewhat better result for B_ϕ than for the magnitude of B_r, which appears to be consistently higher than that observed. The spacecraft data show that the sector boundary of 12 May was complex and included multiple field reversals. It is interesting that B_r exhibits a similar "wave-packet" variation and strongly anticorrelates with u_r on 12 May. In fact, the normalized cross helicity for the B_r and u_r components is nearly maximal, i.e., −1. That might indicate that this large fluctuation is Alfvénic. However, the correlation of the transverse components is not nearly as large, so the fluctuation is not a classical Alfvén wave. In contrast to the complex behavior of the observed magnetic components, the simulated profiles of B_r and B_ϕ are smooth and show only a single current sheet crossing late on 12 May. The computed patterns of M_A and P also appear to agree in general with the observations, but the simulated value of T, while being of right order of magnitude, is clearly out of phase and deviates strongly from the measurements. We believe that the discrepancy in temperature comes from our choice of boundary conditions at 20 $R_\odot$ and a that different condition for temperature could perhaps provide a better fit to the observations.

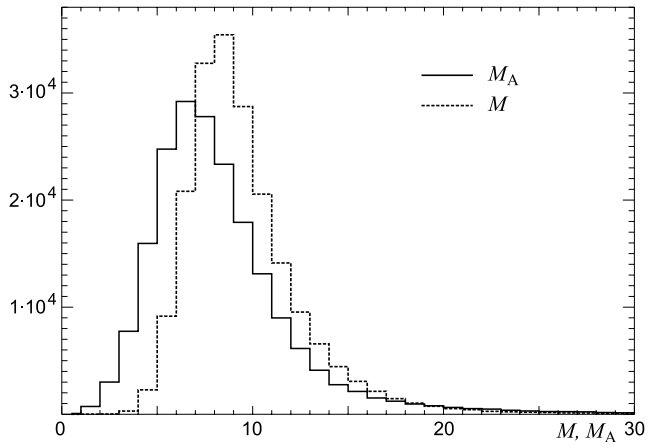

Figure 9. Occurrence rate of the Mach M and Alfvén Mach M_A numbers in the solar wind computed from the hourly OMNI 2 data set for 1963–2003.

4. Low-Density and Sub-Alfvénic Events in the Solar Wind

[24] To gain some insight into the 10–12 May 1999 event in a broader context, in this section we present an outlook of low-density and sub-Alfvénic events which have been observed during last 4 decades. Our analysis differs from similar statistical studies of *Ipavich et al.* [1998] and *Richardson et al.* [2000], as we select only a small number of most prominent events ($n \leq 0.3$ cm^{-3}) and do not restrict ourselves to a particular time interval. Our focus is on sub-Alfvénic events that are mostly a subset of low-density events. Also, in this section we show additional simulations of M_A for the May 1999 transient.

[25] Figure 9 shows occurrence rates of the Mach M and M_A numbers computed using the NSSDC OMNI 2 data set that currently comprises hourly values of interplanetary plasma and magnetic field measurements taken by near-Earth spacecraft from 1963 to 2003. The average values of M and M_A are 9.6 and 8.4, respectively. For the whole space era, we have not found a single example of subsonic flow (the record minimum of $M = 1.87$ was observed on 15 June 1991), but there were 11 events when the solar wind became sub-Alfvénic for a period from 1 to 25 hours. Only one of those events (6 June 1979) was due to an extremely strong magnetic field of 36 nT. The other ten were associated with low-density events, including those of July and November 1979, which were identified and described by *Gosling et al.* [1982] as examples of sub-Alfvénic solar wind [see also *Crooker et al.*, 2000].

[26] To further study the association of low-density events with sub-Alfvénic flows, we scanned through the OMNI 2 spacecraft database and selected all events with abnormally low densities of 0.3 cm^{-3} or smaller. Table 1 presents a list of these 23 events, providing the date and hour of the beginning of the events. Also listed for each event are Carrington rotation number, minimum density ρ_{min} and minimum Alfvén Mach number, M_{Amin}, observed, and the

Table 1. All Events From the OMNI 2 Data Set With $n \leq 0.3$ cm^{-3}

Date	DOY	Hour	CRot	NOP	ρ_{min}	M_{Amin}
1969:03:25	84	21	1545	2	0.2	1.50
1974:05:06	126	22	1614	3	0.2	1.98
1977:10:19	292	20	1660	4	0.3	1.34
1978:09:29	272	19	1673	5	0.2	1.38
1979:07:04	185	8	1683	10	0.04[a]	**0.36**[a]
1979:07:31	212	8	1684	20	0.04[a]	**0.33**[a]
1979:11:22	326	21	1688	4	0.2	**0.90**
1981:10:16	289	14	1714	2	0.3	1.39
1997:02:10	41	8	1919	1	0.3	1.38
1998:05:05	125	7	1935	5	0.3	1.31
1999:04:27	117	2	1948	5	0.3	1.04
1999:05:11	131	5	1949	15	0.1	**0.80**
1999:06:28	179	10	1951	9	0.2	1.86
2000:03:29	89	8	1961	1	0.2	**0.90**
2001:04:30	120	17	1975	2	0.3	2.26
2001:05:31	151	11	1976	2	0.2	1.09
2001:09:08	251	19	1980	5	0.1	**0.92**
2001:11:07	311	7	1982	1	0.3	2.04
2002:03:20	79	12	1987	2	0.2	**0.65**
2002:05:23	143	22	1990	42	0.1	**0.55**
2002:07:19	200	17	1992	6	0.2	**0.82**
2003:02:01	32	15	1999	1	0.3	1.41
2003:07:06	187	21	2005	3	0.2	1.57

[a]These values were inferred from 2-min ISEE-3 data set. That was done because the OMNI 2 densities contained a number of zero values for the two events in 1979, a result of rounding off very small values to fit into a format that allowed only one position after decimal point (J. H. King, private communication, 2004).

number of hourly intervals (NOP) for which $n \leq 0.3$ cm^{-3}. The latter number provides an assessment of the importance of each event and clearly singles out the most outstanding depletions of 1979, 1999, and 2002. Nine of 11 sub-Alfvénic events appear on this list of very low density anomalies; the appropriate M_{Amin} numbers are marked out by boldface in Table 1. One of the events (19 June 2001), which does not appear on the list, took place during a moderate rarefaction of 0.6 cm^{-3} and relatively strong magnetic field of 16 nT. The second one of 6 June 1979 was not accompanied by a noticeable rarefaction and (as mentioned before) was a result of extremely intensive magnetic field.

[27] It is evident from Table 1 that the very low density events reveal a tendency to occur around solar activity maxima. A similar conclusion was drawn by *Richardson et al.* [2000] from their analysis of solar wind events with $n \leq 1$ cm^{-3}. We should note this fact appears to support our hypothesis that low-density events are associated with solar magnetic field restructuring which is especially intense around solar maxima when polar field reversals take place. It is also evident from Table 1 that lower values of ρ_{min} tend to be associated with lower M_{Amin}, which is not surprising as $M_A \sim \rho^{1/2}$. Using data from Table 1, Figure 10 depicts M_{Amin} as a function of ρ_{min} and shows even more clearly that the correlation between M_{Amin} and ρ_{min} is high.

[28] The 10–12 May 1999 event is thus just one of several instances when the solar wind became sub-Alfvénic. In connection with the 22 November 1979 event, *Gosling et al.* [1982] suggested that the flow was sub-Alfvénic at all radial distances from the Sun. Using our simulation results, we can try to investigate this conjecture for the May 1999 event. Figure 11 shows color maps of M_A for t = 64, 128, and 256 hours. There is a visible sub-Alfvénic "tongue" extending outward from the Sun; then it gets disconnected and moves outward embedded in the low-density region.

5. Conclusions

[29] It is evident from this study that the essential features of 10–12 May event (when the Earth was engulfed in solar wind flow of such low density that the event has been referred to "as the day the solar wind disappeared" [*Lazarus*, 2000]) can be successfully reproduced assuming coronal outflow suppression. In this scenario, the solar surface magnetic fields change in such a way that outflow from a region that earlier was a source of fast flow is partially suppressed. We show that a low-density transient forms in front of the slow flow that emerges behind the fast flow. Using a two-dimensional numerical MHD model, we have shown that a very strong rarefaction with an

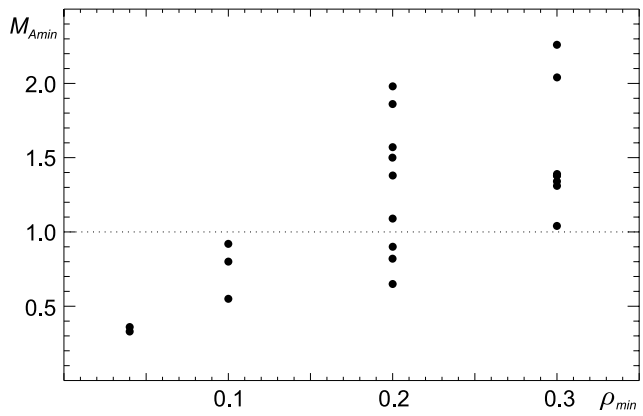

Figure 10. Lowest Alfvén Mach number M_{Amin} versus lowest density ρ_{min}.

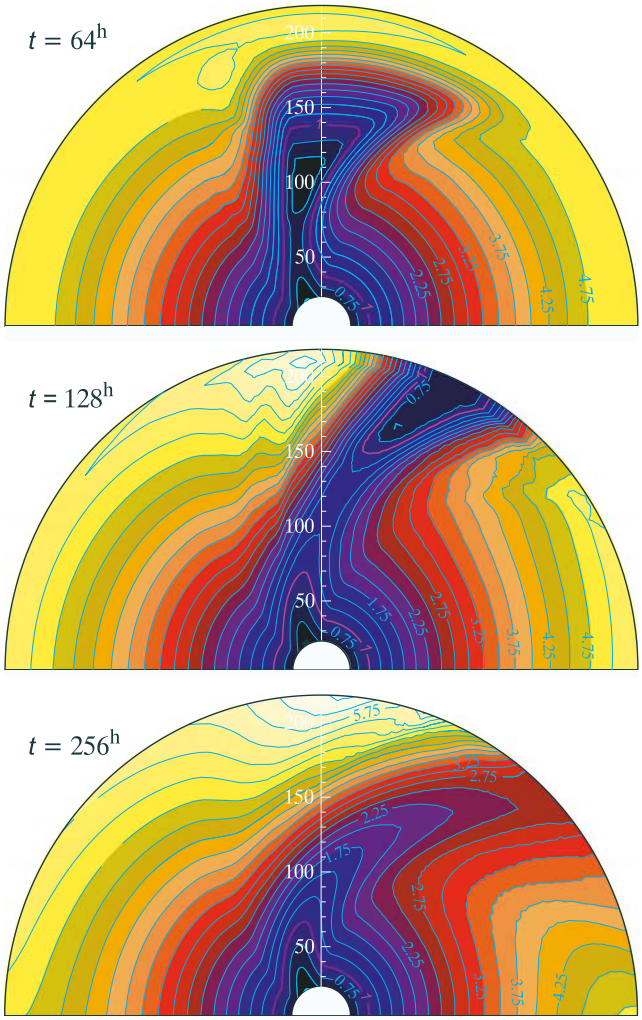

Figure 11. Simulation example: Contour plots of M_A at t = 64, 128, and 256^h. The purple line shows the values of M_A = 1.

embedded sub-Alfvénic region develops on the trailing edge of the fast flow.

[30] For a reasonable choice of plasma and magnetic field parameters close to the Sun, the model appears to be in agreement with the OMNI 2 spacecraft data. In particular, the radial magnetic field shows a relatively small variation across the density anomaly, as observed during May 1999 event. The model also reproduces the strong azimuthal velocities observed in the slow flow region. Our simulation also shows that the flow in the low-density region can be sub-Alfvénic and that the sub-Alfvénic solar wind may not extend back to the Sun but instead gets disconnected as the low-density transient propagates out to the Earth orbit.

[31] In conclusion, we note that these simulations show that strong density depletions may result from a process that suppresses outflow from a region of formerly fast flow, which is opposite to the increase in speed that is characteristic of CMEs. We suspect that such outflow suppressions are not restricted to events of extremely low density but might be a fairly common phenomenon.

[32] **Acknowledgments.** We acknowledge the use of OMNI 2 near-Earth solar wind data supplied by the National Space Science Data Center through the OMNIWeb. This work was performed while one of the authors (AVU) held a National Research Council Senior Research Associateship at the NASA Goddard Space Flight Center.

[33] Shadia Rifai Habbal thanks Hari Om Vats and You-Qiu Hu for their assistance in evaluating this paper.

References

Balasubramanian, V., P. Janardhan, S. Srinivasan, and S. Ananthakrishnan (2003), Interplanetary scintillation observations of the solar wind disappearance event of May 1999, *J. Geophys. Res.*, *108*(A3), 1121, doi:10.1029/2002JA009516.

Crooker, N. U., S. Shodhan, J. T. Gosling, J. Simmerer, R. P. Lepping, J. T. Steinberg, and S. W. Kahler (2000), Density extremes in the solar wind, *Geophys. Res. Lett.*, *27*(23), 3769–3772.

De Young, D. S., and A. J. Hundhausen (1971), Two-dimensional simulation of flare-associated disturbances in the solar wind, *J. Geophys. Res.*, *76*(10), 2245–2253.

Fairfield, D. H., I. H. Cairns, M. D. Desch, A. Szabo, A. J. Lazarus, and M. R. Aellig (2001), The location of low Mach number bow shocks at Earth, *J. Geophys. Res.*, *106*(A11), 25,361–25,376.

Gosling, J. T. (2000), Coronal mass ejections, *Proc. Int. Conf. Cosmic Rays 26th*, 59–79.

Gosling, J. T., and P. Riley (1996), The acceleration of slow coronal mass ejections in the high-speed solar wind, *Geophys. Res. Lett.*, *23*(21), 2867–2870.

Gosling, J. T., and R. M. Skoug (2002), On the origin of radial magnetic fields in the heliosphere, *J. Geophys. Res.*, *107*(A10), 1327, doi:10.1029/2002JA009434.

Gosling, J. T., J. R. Asbridge, S. J. Bame, W. C. Feldman, R. D. Zwickl, G. Paschmann, and N. Sckopke (1982), A sub-Alfvénic solar wind: Interplanetary and magnetosheath observations, *J. Geophys. Res.*, *87*(A1), 239–245.

Groth, C. P. T., D. L. De Zeeuw, T. I. Gombosi, and K. G. Powell (2000), Global three-dimensional MHD simulation of a space weather event: CME formation, interplanetary propagation, and interaction with the magnetosphere, *J. Geophys. Res.*, *105*(A11), 25,053–25,078.

Han, S. M., S. T. Wu, and M. Dryer (1988), A three-dimensional, time-dependent numerical modeling of supersonic, super-Alfvénic MHD flow, *Comp. Fluids*, *16*(1), 81–103.

Hu, Y. Q. (1998), Asymmetric propagation of flare-generated shocks in the heliospheric equatorial plane, *J. Geophys. Res.*, *103*(A7), 14,631–14,641.

Hundhausen, A. J. (1972), *Coronal Expansion and Solar Wind*, Springer, New York.

Hundhausen, A. J., and R. A. Gentry (1969), Numerical simulation of flare-generated disturbances in the solar wind, *J. Geophys. Res.*, *74*(11), 2908–2918.

Ipavich, F. M., et al. (1998), Solar wind measurements with SOHO: The CELIAS/MTOF proton monitor, *J. Geophys. Res.*, *103*(A8), 17,205–17,213.

Lazarus, A. J. (2000), The day the solar wind almost disappeared, *Science*, *287*(5461), 2172–2173.

Manchester, W. B., T. I. Gombosi, I. Roussev, A. Ridley, D. L. De Zeeuw, I. V. Sokolov, and K. G. Powell (2004), Modeling a space weather event from the Sun to the Earth: CME generation and interplanetary propagation, *J. Geophys. Res.*, *109*, A02107, doi:10.1029/2003JA010150.

McComas, D. J., et al. (2000), Solar wind observations over Ulysses' first full polar orbit, *J. Geophys. Res.*, *105*(A5), 10,419–10,433.

Mikić, Z., and J. A. Linker (1994), Disruption of coronal magnetic field arcades, *Astrophys. J.*, *430*, 898–912.

Nakagawa, Y., and R. S. Steinolfson (1976), Dynamical response of the solar corona, I. Basic formulations, *Astrophys. J.*, *207*, 296–299.

Nakagawa, Y., and R. E. Wellck (1973), Numerical studies of azimuthal modulations of the solar wind with magnetic fields, *Solar Phys.*, *32*, 257–270.

Odstrčil, D., and V. J. Pizzo (1999), Three-dimensional propagation of coronal mass ejections (CMEs) in a structured solar wind flow: 1. CME launched within the streamer belt, *J. Geophys. Res.*, *104*(A1), 483–492.

Odstrčil, D., J. A. Linker, R. Lionello, Z. Mikić, P. Riley, V. J. Pizzo, and J. G. Luhmann (2002), Merging of coronal and heliospheric numerical two-dimensional MHD models, *J. Geophys. Res.*, *107*(A12), 1493, doi:10.1029/2002JA009334.

Phillips, J. L., S. J. Bame, W. C. Feldman, J. T. Gosling, D. J. McComas, B. E. Goldstein, and M. Neugebauer (1996), Ulysses solar wind plasma observations from peak southerly latitude through perihelion and beyond, in *Solar Wind Eight*, edited by D. Winterhalter et al., *AIP Conf. Proc.*, *382*, 416–419.

Pizzo, V. J. (1978), A three-dimensional model of corotating streams in the solar wind: 1. Theoretical foundations, *J. Geophys. Res.*, *83*(A12), 5563–5572.

Pneuman, G. W., and R. A. Kopp (1971), Gas-magnetic field interactions in the solar corona, *Solar Phys.*, *18*, 258–270.

Richardson, I. G., D. Berdichevsky, M. D. Desch, and C. J. Farrugia (2000), Solar-cycle variation of low density solar wind during more than three solar cycles, *Geophys. Res. Lett.*, *27*(23), 3761–3764.

Riley, P., J. T. Gosling, and V. J. Pizzo (1997), A two-dimensional simulation of the radial and latitudinal evolution of a solar wind disturbance driven by a fast, high-pressure coronal mass ejection, *J. Geophys. Res.*, *102*(A7), 14,677–14,685.

Smith, C. W., D. J. Mullan, N. F. Ness, R. M. Skoug, and J. Steinberg (2001), Day the solar wind almost disappeared: Magnetic field fluctuations, wave refraction and dissipation, *J. Geophys. Res.*, *106*(A9), 18,625–18,634.

Smith, C. W., D. J. Mullan, and N. F. Ness (2004), Further evidence of wave refraction associated with extended rarefaction events in the solar wind, *J. Geophys. Res.*, *109*, A01111, doi:10.1029/2003JA010113.

Steinolfson, R. S., and M. Dryer (1984), Propagation of solar generated disturbances through the solar wind critical points: One-dimensional analysis, *Astrophys. Space Sci.*, *104*, 111–120.

Tóth, G. (2000), The $\nabla \cdot B = 0$ constraint in shock-capturing magnetohydrodynamics codes, *J. Comput. Phys.*, *161*, 605–652.

Tóth, G., and D. Odstrčil (1996), Comparison of some flux corrected transport and total variation diminishing numerical schemes for hydrodynamic and magnetohydrodynamic problems, *J. Comput. Phys.*, *128*(2), 82–100.

Totten, T. L., J. W. Freeman, and S. Arya (1995), An empirical determination of the polytropic index for the free-streaming solar wind using Helios 1 data, *J. Geophys. Res.*, *100*(A1), 13–17.

Usmanov, A. V. (1993), A global numerical 3-D MHD model of the solar wind, *Solar Phys.*, *146*, 377–396.

Usmanov, A. V., and M. Dryer (1995), A global 3-D simulation of interplanetary dynamics in June 1991, *Solar Phys.*, *159*, 347–370.

Usmanov, A. V., M. L. Goldstein, B. P. Besser, and J. M. Fritzer (2000a), A global MHD solar wind model with WKB Alfvén waves: Comparison with Ulysses data, *J. Geophys. Res.*, *105*(A6), 12,675–12,695.

Usmanov, A. V., M. L. Goldstein, and W. M. Farrell (2000b), A view of the inner heliosphere during the May 10–11, 1999 low density anomaly, *Geophys. Res. Lett.*, *27*(23), 3765–3768.

Vats, H. O., H. S. Sawant, R. Oza, K. N. Iyer, and R. Jadhav (2001), Interplanetary scintillation observations for the solar wind disappearance event of May 1999, *J. Geophys. Res.*, *106*(A11), 25,121–25,124.

Weber, E. J., and L. Davis (1967), The angular momentum of the solar wind, *Astrophys. J.*, *148*, 217–227.

Wu, S. T., M. Dryer, and S. M. Han (1983), Non-planar MHD model for solar flare-generated disturbances in the heliospheric equatorial plane, *Solar Phys.*, *84*, 395–418.

Wu, S. T., W. P. Guo, D. J. Michels, and L. F. Burlaga (1999), MHD description of the dynamical relationships between a flux rope, streamer, coronal mass ejection, and magnetic cloud: An analysis of the January 1997 Sun-Earth connection event, *J. Geophys. Res.*, *104*(A7), 14,789–14,801.

W. M. Farrell, Code 695, NASA Goddard Space Flight Center, Greenbelt, MD 20771, USA. (william.m.farrell@nasa.gov)

M. L. Goldstein and A. V. Usmanov, Code 692, NASA Goddard Space Flight Center, Greenbelt, MD 20771, USA. (melvyn.l.goldstein@nasa.gov; usmanov@geo.phys.spbu.ru)

G. R. Lawrence, Department of Solar Physics, Royal Observatory of Belgium, B-1180 Brussels, Belgium. (gareth.lawrence@oma.be)

K. W. Ogilvie, Code 690.4, NASA Goddard Space Flight Center, Greenbelt, MD 20771, USA. (keith.w.ogilvie@nasa.gov)